New EU data regulations, global research implications *pp. 467 & 496*

Sexual harassment allegations roil the Salk Institute *p. 480*

Targets for malaria mutagenesis *pp. 490 & 506*

Science

$15
4 MAY 2018
sciencemag.org

AAAS

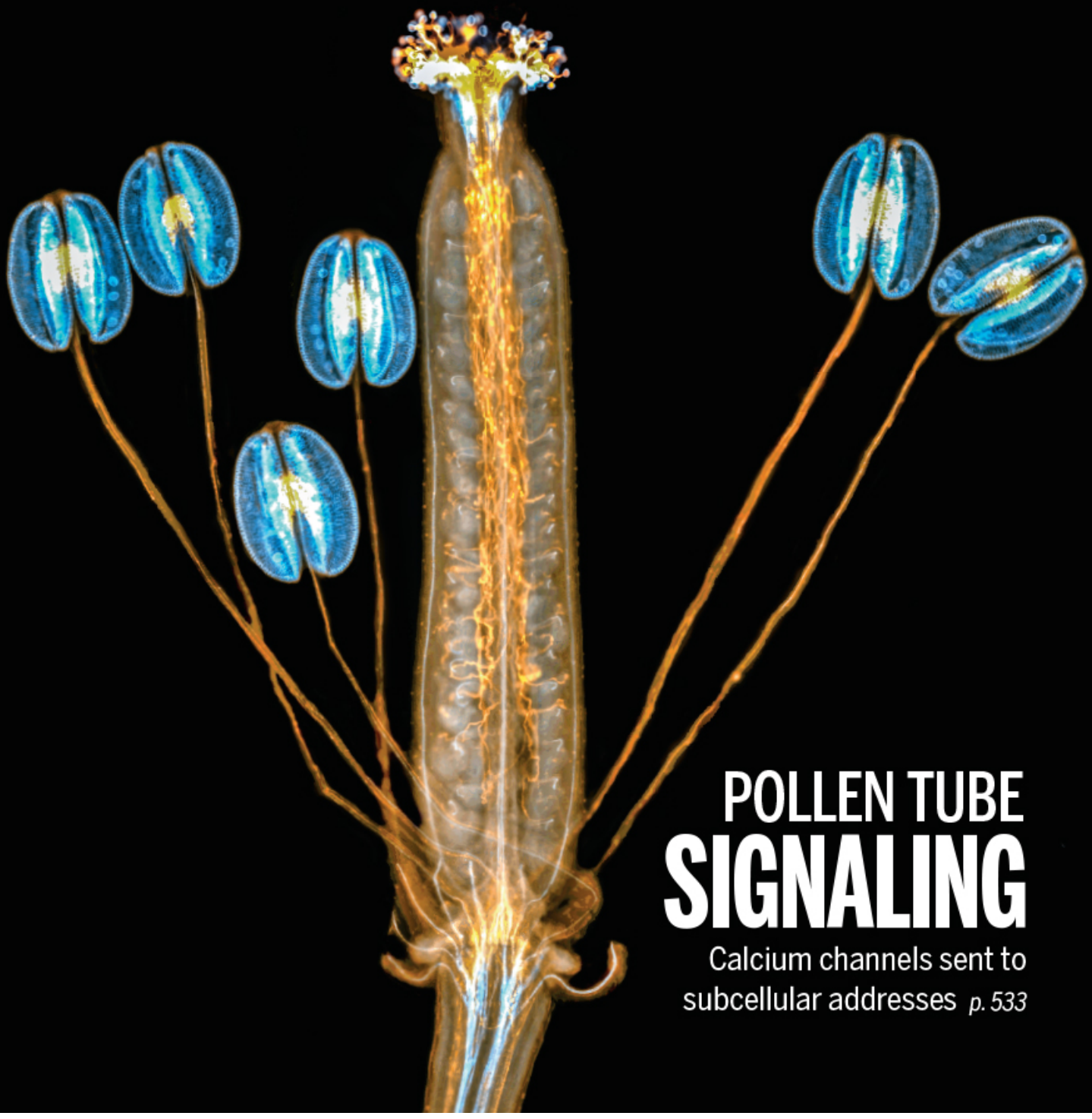

POLLEN TUBE SIGNALING

Calcium channels sent to subcellular addresses *p. 533*

PLANT SCIENCE

CORNICHON sorting and regulation of GLR channels underlie pollen tube Ca^{2+} homeostasis

Michael M. Wudick,[1,2] Maria Teresa Portes,[1,2] Erwan Michard,[1,2] Paul Rosas-Santiago,[3] Michael A. Lizzio,[1] Custódio Oliveira Nunes,[1,2] Cláudia Campos,[2] Daniel Santa Cruz Damineli,[1] Joana C. Carvalho,[2] Pedro T. Lima,[2] Omar Pantoja,[3] José A. Feijó[1,2]*

Compared to animals, evolution of plant calcium (Ca^{2+}) physiology has led to a loss of proteins for influx and small ligand–operated control of cytosolic Ca^{2+}, leaving many Ca^{2+} mechanisms unaccounted for. Here, we show a mechanism for sorting and activation of glutamate receptor–like channels (GLRs) by CORNICHON HOMOLOG (CNIH) proteins. Single mutants of pollen-expressed *Arabidopsis thaliana* GLRs (*At*GLRs) showed growth and Ca^{2+} flux phenotypes expected for plasma membrane Ca^{2+} channels. However, higher-order mutants of *At*GLR3.3 revealed phenotypes contradicting this assumption. These discrepancies could be explained by subcellular *At*GLR localization, and we explored the implication of *At*CNIHs in this sorting. We found that *At*GLRs interact with *At*CNIH pairs, yielding specific intracellular localizations. *At*CNIHs further trigger *At*GLR activity in mammalian cells without any ligand. These results reveal a regulatory mechanism underlying Ca^{2+} homeostasis by sorting and activation of *At*GLRs by *At*CNIHs.

Plants use Ca^{2+} signaling despite lacking many components known to control the cytosolic Ca^{2+} concentration in mammalian cells (*1*). The gene family encoding glutamate receptor–like channels (GLRs) has been implicated in Ca^{2+} transport in various settings, namely, male gamete function (*2*, *3*), stomatal closure (*4*), immunity (*5*), wound signaling (*6*), and root initiation (*7*). Evolutionary diversification of this family in Arabidopsis (*AtGLR*) resulted in 20 genes, distributed into three clades (*8*). To study *AtGLR* function in pollen tubes, whose growth and function depend on Ca^{2+} influx (*9*), we used reverse genetics, generating multiple *AtGLR* mutants (fig. S1, A and B).

In general, pollen tubes carrying *At*GLR mutations showed conspicuous branching (Fig. 1, A to D), preceded by emergence of a new Ca^{2+} gradient, which reestablished the gradient onto the growing tip (Fig. 1, F and G, and movie S1). We also observed that sperm cells were typically shunted into the growing branch (Fig. 1E), suggesting that tip Ca^{2+} signaling established growth polarity and guided sperm nuclei toward the growing tip, thereby providing a basis for the unaffected fertility of most mutants.

We measured extracellular net Ca^{2+} fluxes of growing pollen tube tips using a Ca^{2+}-selective vibrating probe. Tubes from *glr1.2*, *glr2.1*, *glr1.1/glr1.2*, *glr1.2/glr1.4-1*, and *glr1.2/1.4-1/2.2/3.3-1* mutants showed only half the flux of wild type (Fig. 1H, lower panel). Lower cytosolic Ca^{2+} concentrations in tip and shank were found in *glr1.1/glr1.2* tubes (Fig. 1I) as quantified with the ratiometric Ca^{2+} sensor Yellow Cameleon 3.6 (YC3.6) (*2*, *10*), supporting the view of *At*GLRs as plasma membrane channels (*1*). Additionally, *glr1.2/glr1.4* pollen tubes were shorter than those of wild type (~100 μm; Fig. 1J and fig. S2A), suggesting that mutations in *AtGLR*s affect various pollen-mediated phenotypes. Mutations that did not alter Ca^{2+} fluxes often experienced genetic compensation. For instance, in *glr1.1/1.4-1* pollen, *AtGLR1.2* mRNA was overexpressed (fig. S1C).

A diminished growth rate did not correlate with Ca^{2+} flux reductions. Double and triple mutants involving *AtGLR3.3* showed greater Ca^{2+} fluxes than mutants not involving *AtGLR3.3*. Whereas *glr1.2* alone decreased Ca^{2+} flux, the *glr1.2/3.3* double mutant restored it. Nonetheless, in all mutant combinations, pollen tubes grew more slowly than wild type (Fig. 1H, upper panel). Thus, a correlation between Ca^{2+} influx and growth (*11*) did not hold. Cluster analysis revealed a group of mutants with wild-type or higher Ca^{2+} fluxes but slower-than-normal growth rates, composed of double or triple mutants that include *AtGLR3.3* (fig. S2B). We defined a "Ca^{2+} use growth efficiency" metric as the ratio of growth rate to Ca^{2+} flux (Fig. 1K). In mutants involving *glr3.3*, this efficiency decreased as a result of high fluxes, and we hypothesized that mechanisms other than channel conductance could regulate Ca^{2+} homeostasis.

So far, *At*GLRs, like their mammalian counterparts, have been assumed to localize to the plasma membrane (*1*, *7*). However, the antagonistic effects of *glr1.2* and *glr3.3* could be explained by their localization in different membranes. Therefore, we analyzed the subcellular localization of *At*GLR3.3 and *At*GLR2.1, the *At*GLR most highly expressed in pollen. *At*GLR2.1-GFP (green fluorescent protein) localized to the complex vacuolar system (Fig. 2A and fig. S2, C to F), whereas *At*GLR3.3-GFP localized to the sperm plasma membrane and endomembranes but was undetectable in the pollen tube plasma membrane (Fig. 2B and fig. S2, G to I), indicating that the secretory pathway must sort and target both *At*GLRs.

We queried a membrane-based interactome database (*12*) for *CORNICHON* homologs, because they mediate the trafficking of ionotropic glutamate receptors (iGluRs) in animal cells (*13*). Arabidopsis contains five *CORNICHONS* (*AtCNIH1-5*; fig. S3, A and D). *At*CNIH1 interacted with various *At*GLRs (*12*). *At*CNIH1-5 all share characteristic features, including a *cornichon* motif (fig. S3, A and B) and an "IFRTL"-like Sec24-interacting motif (fig. S3, A, B, E, and F). RNA of all *AtCNIHs* was detected in pollen, being highest for *AtCNIH4* (fig. S3C). Both *At*CNIH1 and *At*CNIH4 interact with *At*GLR3.3 (Fig. 2C). In other species, CORNICHONS are essential for sorting and trafficking proteins from the endoplasmic reticulum (ER). We confirmed this for *At*CNIHs by complementing the *erv14p*Δ yeast *Saccharomyces cerevisiae* (*Sc*) CORNICHON mutant (*14*) and observing tolerance toward Na^+ and *Sc*Nha1p localization (Fig. 2F and fig. S3G). Plasma membrane localization of *Sc*Nha1p in the *erv14p*Δ mutant was rescued by *At*CNIH1, 3, and 4, but not by *At*CNIH2 or 5, and restored Na^+ tolerance to wild-type levels, permitting growth on 800 mM NaCl.

In pollen, red fluorescent protein–tagged *At*CNIHs (RFP-*At*CNIHs) localized to endomembranes and punctate structures (Fig. 2, D and E, and fig. S4, A to C) that colocalized with markers for the ER (fig. S4, L to S) but not the cis or medial Golgi (fig. S4, D to K). We also observed pollen tube plasma membrane localization of RFP-*At*CNIH4 (Fig. 2E) and RFP-*At*CNIH3 (fig. S4C). The presence of *At*CNIHs in ER foci (Fig. 2, D and E) was consistent with their localization at ER exit sites (ERES) (*15*). Indeed, *At*CNIHs colocalized with the ERES marker *At*Sec24 (fig. S4, T to W). *cnih1*, *cnih4*, and the double *cnih1/cnih4* mutants (fig. S5, A and B) showed reduced pollen tube tip Ca^{2+} fluxes but wild-type–like growth rates (fig. S5, C and D).

We next analyzed the impact of *At*CNIHs on cargo trafficking. Although *At*GLR3.3-GFP localized to sperm in *cnih1* or *cnih4* pollen (Fig. 3, A and B), it accumulated in reticulate and punctate structures in *cnih1/cnih4* (Fig. 3C) and other *cnih* double mutants (fig. S6, A to E). Neither overexpression of *At*GLR3.3-GFP in *cnih1* and *cnih4* pollen, nor its endomembrane retention in *cnih1/cnih4* mutants, changed the Ca^{2+} flux phenotypes observed in corresponding lines lacking *At*GLR3.3-GFP (fig. S7A). Confirming a role in ER sorting, *At*GLR2.1-GFP was similarly retained in endomembranes in *cnih1/cnih4*, but not in any single mutant (fig. S6, F to H).

We next addressed the *At*CNIH cargo specificity in wild type and *cnih1/cnih4* by comparing two P-type ATPases (adenosine triphosphatases) with comparable intramembrane domain topology.

[1]University of Maryland Department of Cell Biology and Molecular Genetics, 0118 Bioscience Research Building, 4066 Campus Drive, College Park, MD 20742-5815, USA. [2]Instituto Gulbenkian de Ciência, Rua da Quinta Grande 6, Oeiras, 2780-156, Portugal. [3]Instituto de Biotecnología, Universidad Nacional de Autónoma de México, Cuernavaca, Morelos 62250, México.
***Corresponding author. Email: jfeijo@umd.edu**

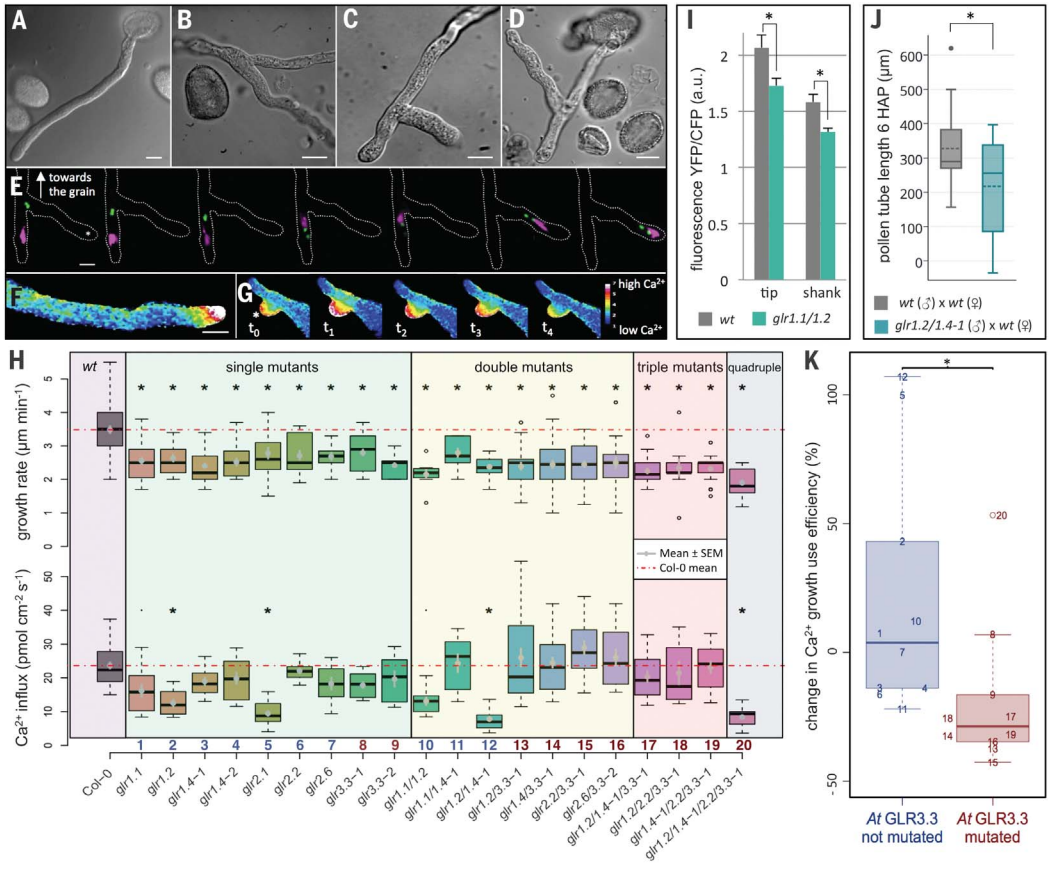

Fig. 1. Characterization of *At*GLR loss-of-function lines. Differential interference contrast images of wild-type (**A**), *glr1.4-1* (**B**), *glr3.3-1* (**C**), and *glr1.4-1/3.3-1* (**D**) pollen. (**E**) Time-lapse series of migrating vegetative (magenta) and sperm (green) nuclei in a branching *glr3.3-1* tube. The tube outline is dotted; the asterisk indicates the growing branch. (**F**) Steep Ca^{2+} gradient in an YC3.6-expressing wild-type pollen tube with highest Ca^{2+} concentration ($[Ca^{2+}]$) at the tip. (**G**) Time series (t_0 to t_4, movie S1) of a branching YC3.6-expressing *glr1.4-1* tube with oscillatory $[Ca^{2+}]$ at the newly emerging tip (asterisk). Bars, 10 µm. (**H**) Pollen tube growth rate (upper panel) and Ca^{2+} influx (lower panel) across the tip plasma membrane of wild-type (Col-0) and *glr* mutants. Dot-dashed lines represent wild-type means of growth rate or Ca^{2+} influx, respectively. $^*P < 0.05$, $\cdot P < 0.1$. (**I**) YC3.6-measured cytosolic Ca^{2+} signatures (YFP/CFP fluorescence values) were significantly lower in *glr1.1/1.2* than in wild type, both at the tip ($^*P < 0.05$) and shank ($^*P < 0.05$). (**J**) Average length of wild-type and *glr1.2/glr1.4-1* pollen tubes 6 hours after pollination (HAP, $n = 15$) on wild-type pistils. Asterisk indicates significant difference from wild type ($P < 0.05$); dotted line represents mean. (**K**) Comparison of normalized growth rates/fluxes, in mutants with (*At*GLR3.3 not mutated) or without *At*GLR3.3 (*At*GLR3.3 mutated). Numbers refer to the lines in Fig. 1H. $^*P < 0.01$.

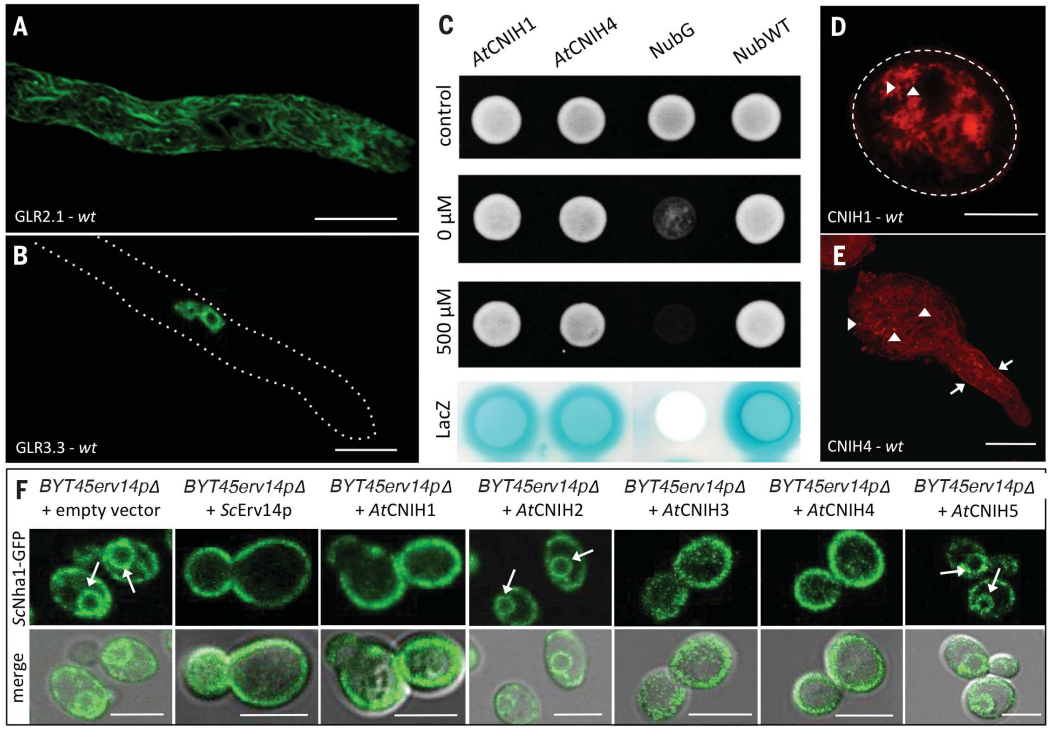

Fig. 2. Subcellular localization of *At*GLRs and *At*CNIHs, their interaction, and functional yeast complementation. Wild-type (*wt*) pollen tubes expressing *At*GLR2.1-GFP (**A**) or *At*GLR3.3-GFP (**B**) localizing to the tonoplast or sperm cell plasma membrane and endomembranes, respectively. Tube contour indicated by dotted line. (**C**) Yeast mating-based split ubiquitin system (mbSUS) assay revealing interaction on control (row 1) or selective media (rows 2 and 3) of *At*GLR3.3/*At*CNIH1 (column 1) or *At*CNIH4 (column 2) in the absence (0 µM) or presence (500 µM) of methionine. Negative (NubG) and positive controls (NubWT) are in columns 3 and 4, respectively. *At*GLR3.3/*At*CNIH1 and *At*GLR3.3/*At*CNIH4 interactions were corroborated by *LacZ* activation (bottom row). (**D**) RFP-*At*CNIH1 and (**E**) RFP-*At*CNIH4 labeling ER exit site–like structures (ERES, arrowheads), and the tube plasma membrane [(E), arrows]. Bars, 10 µm. (**F**) Fluorescence (upper row) and merged bright-field images (lower row) of an *BYT45ervp*Δ yeast expressing *Sc*Nha1p-GFP and cotransformed with the *At*CNIHs. Arrows indicate the peri-nuclear ER. Bars, 5µm.

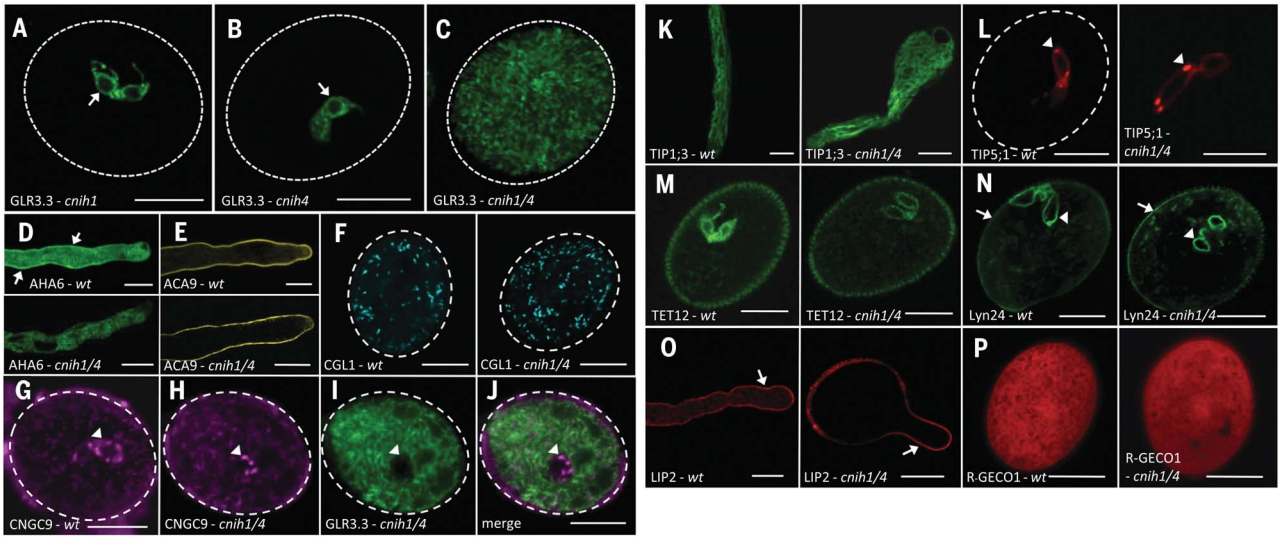

Fig. 3. Expression of *At*GLR3.3-GFP and reference proteins in control and *cnih* pollen. (**A**) *cnih1* and (**B**) *cnih4* pollen expressing *At*GLR3.3-GFP in sperm cells (arrows). (**C**) *At*GLR3.3-GFP localization in *cnih1/cnih4* pollen, labeling endomembranes. (**D**) Expression of *At*AHA6-GFP or (**E**) *At*ACA9-YFP in wild-type (*wt*, upper panels) or *cnih1/cnih4* pollen (lower panels). (**F**) Localization of the cis or medial Golgi marker *At*CGL1-CFP in wild-type (*wt*, left panel) and *cnih1/cnih4* pollen (right panel). Expression of mCherry-*At*CNGC9 in wild-type (*wt*) (**G**) or *cnih1/cnih4* pollen (**H**) coexpressing *At*GLR3.3-GFP (**I**). (**J**) Corresponding merged image. (**K**) Expression of *At*TIP1;3-GFP, (**L**) *At*TIP5;1-mCherry, (**M**) *At*TET12-GFP, (**N**) *Mus musculus* Lyn24 (*Mm*Lyn24-GFP), (**O**) *At*LIP2-RFP, and (**P**) R-GECO1 in wild-type (*wt*, left panels) and *cnih1/cnih4* pollen (right panels). Arrows indicate the tube plasma membrane, arrowheads the sperm cells. Bars, 10 μm.

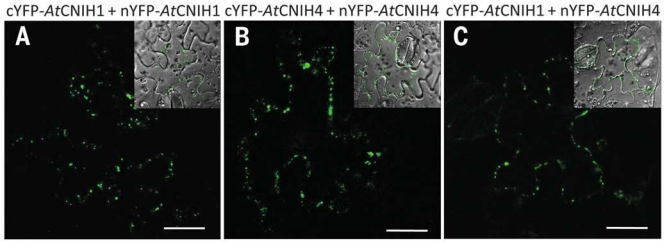

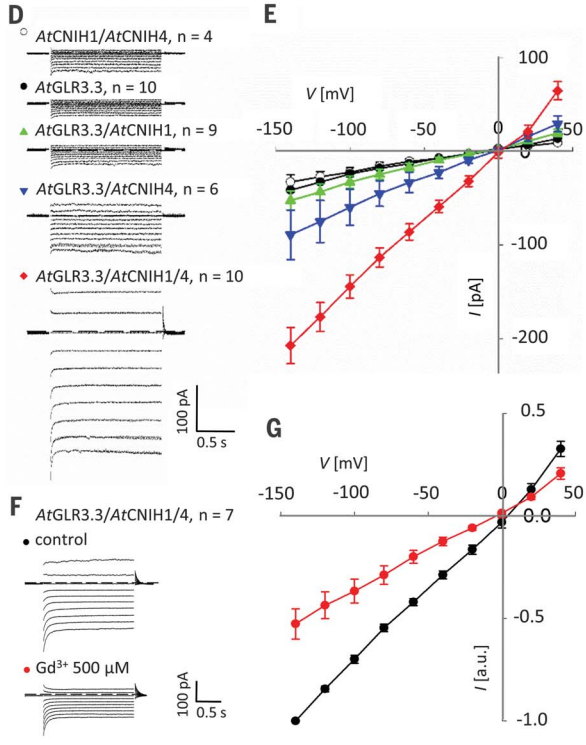

Fig. 4. Interaction of *At*CNIH1/*At*CNIH4 and their effect on *At*GLR3.3 current properties. Transient tobacco epidermis leaf expression of cYFP-*At*CNIH1 + nYFP-*At*CNIH1 (**A**) and cYFP-*At*CNIH4 + nYFP-*At*CNIH4 (**B**) caused YFP fluorescence reconstitution, indicating the formation of homomers (A and B) or heteromers (**C**). Insets represent merged bright-field/fluorescence images. Bars, 20 μm. (**D**) Typical currents in COS-7 cells expressing *At*CNIHs, *At*GLR3.3, or a combination thereof. (**E**) Stationary current/voltage relationships from recordings shown in (D). (**F**) Typical currents recorded in cells coexpressing *At*GLR3.3 and *At*CNIH1/*At*CNIH4 in bath solution (control) or after Gd^{3+} addition (Gd^{3+} 500 μM). (**G**) Stationary normalized current/voltage relationships from recordings shown in (F). Error bars represent SE.

Similarly to *At*GLR2.1 and 3.3, the autoinhibited H^+-ATPase 6 (*At*AHA6-GFP) was retained in endomembranes in *cnih1/cnih4* (Fig. 3D), whereas the autoinhibited Ca^{2+}-ATPase 9 (*At*ACA9-YFP) was unaffected in this (Fig. 3E) or other *cnih* double mutants (fig. S6, I and J), suggesting cargo specificity for pairs of *At*CNIHs. Indeed, marker proteins for the cis or medial Golgi (Fig. 3, F to J, and fig. S6, K to M), vegetative and sperm vacuoles (Fig. 3, K and L), and coat protein complex II (COPII) vesicles (fig. S6, N and O) remained correctly targeted in *cnih1/cnih4* pollen, as were proteins with *At*GLR3.3-like localization (Fig. 3, M to O), or a cytoplasmic protein (Fig. 3P). Thus, ER sorting of certain integral membrane proteins, but not of other soluble or membrane-attached proteins, was dependent on *At*CNIH pairs. Although we found that *At*CNIH homomers may be formed (Fig. 4, A and B), *At*GLR trafficking was dependent on the formation of *At*CNIH heteromers (Fig. 4C and fig. S6, P to R).

We next challenged *At*CNIH regulation of *At*GLR channel activity, as documented for animal glutamate receptors (*13*). Patch-clamp experiments in COS-7 cells expressing *At*CNIH1, *At*CNIH4, *At*GLR3.3, or *At*CNIH1/*At*GLR3.3 revealed control-like currents (Fig. 4, D and E, and fig. S7B). However, cells coexpressing *At*GLR3.3/*At*CNIH4 showed larger currents, and coexpression of *At*GLR3.3/*At*CNIH1/*At*CNIH4 led to a twofold increase, even without ligand (Fig. 4, D and E). Currents were ohmic-like, Gd^{3+}-sensitive, and without selectivity for Na^+ over Ca^{2+}, as revealed by the reversal potential close to 0 mV, despite asymmetric solutions (pipette: 150 mM Na^+; bath: 20 mM Ca^{2+}, 10 mM Na^+; Fig. 4, E to G). We next addressed *At*CNIH specificity for eliciting currents by using *At*GLR3.2, a pollen tube–expressed *At*GLR3.3 homolog. Coexpressing *At*GLR3.2 with either *At*CNIH1 or *At*CNIH4 yielded activation of currents similar to those for *At*GLR3.3/*At*CNIH1/*At*CNIH4 (fig. S7, C to F), albeit up to fivefold higher than the currents measured for any other *At*GLR in heterologous systems (*7*, *16*). In COS-7, *At*GLR3.2 plasma membrane localization was independent of *At*CNIH1 or 4 (fig. S7, G to H), suggesting they were more relevant for channel activity than targeting in this system.

We conclude that *At*CNIHs are essential for sorting, trafficking, and localizing *At*GLRs in planta, and the interaction between proteins of these two families enhances *At*GLR channel activity. These additive effects support increased cationic currents driven by *At*GLRs at a magnitude not previously observed (*2*, *7*, *16*). Ionic selectivity of *At*GLRs is not understood, but *Physcomitrella patens* GLR1 (*Pp*GLR1) conducts Ca^{2+} (*3*). Multiple mechanisms linked to cytosolic Ca^{2+} homeostasis may contribute to the phenotypes that we observed. Some *At*GLR members, like *At*GLR1.2, may work as plasma membrane Ca^{2+} channels, but we posit that sorting of other *At*GLRs to internal Ca^{2+} reservoirs (ER, vacuole, mitochondria) contributes to cytosolic Ca^{2+} homeostasis. When perturbed by multiple mutations, Ca^{2+} homeostasis is disrupted and growth is affected. Therefore, our results suggest that specific *At*CNIHs regulate quantity, location, and activity of *At*GLRs, affecting the concentration of cytosolic Ca^{2+} and, by interacting with other protein families, possibly the concentration of different ions (*15*).

REFERENCES AND NOTES

1. K. H. Edel, E. Marchadier, C. Brownlee, J. Kudla, A. M. Hetherington, *Curr. Biol.* **27**, R667–R679 (2017).
2. E. Michard *et al.*, *Science* **332**, 434–437 (2011).
3. C. Ortiz-Ramírez *et al.*, *Nature* **549**, 91–95 (2017).
4. D. Kong *et al.*, *Cell Reports* **17**, 2553–2561 (2016).
5. M. Kwaaitaal, R. Huisman, J. Maintz, A. Reinstädler, R. Panstruga, *Biochem. J.* **440**, 355–365 (2011).
6. S. A. R. Mousavi, A. Chauvin, F. Pascaud, S. Kellenberger, E. E. Farmer, *Nature* **500**, 422–426 (2013).
7. E. D. Vincill, A. E. Clarin, J. N. Molenda, E. P. Spalding, *Plant Cell* **25**, 1304–1313 (2013).
8. R. Davenport, *Ann. Bot.* **90**, 549–557 (2002).
9. E. Michard, A. A. Simon, B. Tavares, M. M. Wudick, J. A. Feijó, *Plant Physiol.* **173**, 91–111 (2017).
10. D. S. C. Damineli, M. T. Portes, J. A. Feijó, *J. Exp. Bot.* **68**, 3267–3281 (2017).
11. J. A. Feijó *et al.*, *BioEssays* **23**, 86–94 (2001).
12. A. M. Jones *et al.*, *Science* **344**, 711–716 (2014).
13. S. C. Haering, D. Tapken, S. Pahl, M. Hollmann, *Membranes* **4**, 469–490 (2014).
14. J. Powers, C. Barlowe, *Mol. Biol. Cell* **13**, 880–891 (2002).
15. P. Rosas-Santiago *et al.*, *J. Exp. Bot.* **66**, 2733–2748 (2015).
16. D. Tapken *et al.*, *Sci. Signal.* **6**, ra47 (2013).

ACKNOWLEDGMENTS

We thank L. Boavida, F. Brandizzi, A. Costa, U. Grossniklaus, J. Harper, M. Iwano, I. Heilmann, M. Palmgren, L.-J. Qu, and Y. Zhang for sharing materials; S. Wolniak and N. Andrews for sharing facilities; A. Beaven for assisting image acquisition; A. David and T. Maié for lab help; L. Boavida for discussions; and A. A. Simon for reviewing the manuscript. **Funding:** NSF (MCB 1616437/2016 and MCB1714993/2017), UMD, and FCT (PTDC/BEX-BCM/0376/2012, PTDC/BIA-PLA/4018/2012) to J.A.F.; CONACYT (220085) and DGAPA-UNAM (IN-203817) to O.P.; and postdoctoral fellowships SFRH/PD/70739/2010 and SFRH/PD/70820/2010 to M.M.W. and M.T.P., respectively.

Author contributions: M.M.W. contributed to the conceptualization, methodology, validation, formal analysis, investigation, resources, data curation, writing, editing, supervision, and vizualization. M.T.P. and E.M. contributed to the methodology, validation, formal analysis, investigation, data curation, writing, reviewing, and visualization. P.R.-S. contributed to the methodology, validation, investigation, resources, reviewing, and visualization. M.A.L. contributed to the methodology, investigation, resources, reviewing, and visualization. C.C. contributed to the methodology, investigation, resources, and review. C.O.N., J.C.C., and P.T.L. contributed to the methodology, validation, investigation, and review. D.S.C.D. contributed to the conceptualization, methodology, software, validation, formal analysis, data curation review, and visualization. O.P. contributed to methodology, review, supervision, and funding aquisition. J.A.F. contributed to the conceptualization, methodology, writing, editing, supervision, project administration, and funding aquisition. **Competing interests:** None declared. **Data and materials availability:** Accession numbers for all genes referred to in this manuscript and all data needed to evaluate the conclusions in the paper are present in the paper or the supplementary materials.

SUPPLEMENTARY MATERIALS

www.sciencemag.org/content/360/6388/533/suppl/DC1
Materials and Methods
Supplementary Text
Figs. S1 to S7
Table S1
Movie S1
References (*17*–*47*)

4 December 2017; accepted 14 March 2018
10.1126/science.aar6464

Science

CORNICHON sorting and regulation of GLR channels underlie pollen tube Ca^{2+} homeostasis

Michael M. Wudick, Maria Teresa Portes, Erwan Michard, Paul Rosas-Santiago, Michael A. Lizzio, Custódio Oliveira Nunes, Cláudia Campos, Daniel Santa Cruz Damineli, Joana C. Carvalho, Pedro T. Lima, Omar Pantoja and José A. Feijó

Science **360** (6388), 533-536.
DOI: 10.1126/science.aar6464

Multiple, diverse, and complex

Calcium currents characterize the developing pollen tube in the small mustard plant *Arabidopsis* and correlate with growth at the tip of the pollen tube. This system constitutes a practical model for screening for Ca^{2+}-signaling mechanisms in plants. Wudick *et al.* analyzed multiple variants of glutamate receptor–like (GLR) channels and discovered that some work alone and others work in pairs or trios. Subcellular localization of GLRs is a complex response to CORNICHON sorting proteins, which leave some GLRs at the plasma membrane and ferry others to internal calcium reservoirs. The calcium current at the tip of the growing pollen tube apparently integrates multiple intracellular currents.

Science, this issue p. 533

POLLEN

Calcium channel helpers

Science **360**, 533–536 (2018)

Credit: Heiti Paves / Alamy Stock Photo

Glutamate is an important neurotransmitter in vertebrates. Its perception across synapses is mediated by transmembrane receptors. Plants also contain glutamate receptor-like (GLR) proteins, which function as non-specific channels with calcium permeability and have been involved in many biological processes, from immunity to metabolism. José Feijó and colleagues have identified molecular partners that are needed for proper function and subcellular localization of GLRs during pollen tube growth.

Arabidopsis contains 20 GLRs. A close inspection of individual and higher-order mutants for pollen-expressed GLRs suggested that their role is more complex than simple plasma membrane calcium channels. A few of them could regulate calcium homeostasis in pollen by redirecting the ion away from the cytosol and into intracellular reservoirs, which implies specific subcellular localizations.

Using analogy with animal systems, the authors focused on the CORNICHON (CNIH) family of proteins needed for trafficking of GLRs in vertebrates. Indeed, in a double *cnih* mutant, GLRs — but not other similarly targeted proteins, indicating some specificity — are not correctly sorted and end up trapped in the endomembrane network. Furthermore, the presence of CNIH proteins increases the GLR ion channel activity, even without its ligand, in electrophysiology assays.

This study shows that understanding biological functions is a fascinating never-ending game of molecular Russian nesting dolls, with many layers of complexity adding on top of each other: calcium is a necessary signal for pollination, GLRs modulate calcium fluxes, CNIH controls GLR localization and activity. Now may be the time to address how CNIH proteins are regulated.

Guillaume Tena

Published online: 4 June 2018
https://doi.org/10.1038/s41477-018-0184-z